Nanoimprinted SERS-Active Substrates with Tunable Surface Plasmon Resonances

Ramon Alvarez-Puebla,[†] Bo Cui,[‡] Juan-Pablo Bravo-Vasquez,[†] Teodor Veres,*[,‡] and Hicham Fenniri*[,†,§]

National Institute for Nanotechnology, National Research Council, 11421 Saskatchewan Drive, Edmonton, Alberta T6G 2M9, Canada, Industrial Material Institute, National Research Council, 75 Boulevard de Mortagne, Boucherville, Quebec J4B 6Y4, Canada, and Gunning/Lemieux Chemistry Center, University of Alberta, 11227 Saskatchewan Drive, Edmonton, Alberta T6G 2G2, Canada

Received: February 1, 2007; In Final Form: March 12, 2007

Nanoimprint lithography and physical vapor deposition were combined to fabricate large-area homogeneously patterned SERS-active substrates with tunable surface plasmon resonances. The plasmon shift observed was connected to the surface nanotopography since (a) the SERS-active nanoparticles on all the substrates investigated were shown to be chemically and structurally similar and (b) the SERS spectra of the analyte investigated were essentially identical for all samples. In addition, the tunability of surface nanotopography was shown to boost the SERS effect via optimal coupling between the substrate's SPR and the incident laser line.

Introduction

Surface plasmon resonance (SPR), the collective oscillation of the conduction electrons in metal nanostructures, is the object of intense multidisciplinary research with a wide scope of bioanalytical applications.[1,2] Correlation between SPR and surface-enhanced Raman scattering (SERS) has been theoretically[3] and experimentally[4,5] demonstrated by using surface-enhanced Raman excitation spectroscopy (SERES).[3,6,7] To maximize the SERS signals, enhance the reproducibility, and expand the applicability of this analytical technique in ultrasensitive detection,[8,9] optimization of the correlation between the surface plasmon resonance and the excitation laser line is necessary.[10,11] To achieve these goals, nanopatterned substrates with precisely defined surface features were fabricated with use of e-beam nanolithography (EBL)[12] and nanosphere lithography (NSL).[13,14] However, EBL is time-consuming, and not amenable to large-scale production, whereas NSL is limited in terms of structures and topographies generated.

To overcome some of these limitations, we combined nanoimprint lithography (NIL)[15] and physical vapor deposition (PVD) to fabricate five large-area homogeneously patterned SERS-active substrates with tunable SPR. Investigation of the SERS properties of these substrates relative to flat silver films showed a significantly large, topographically dependent enhancement, which was correlated with the substrate's SPR.

Experimental Methods

Grating and pillar films were prepared by NIL in accordance with Chou's method,[15] using a thin layer (200 nm) of polystyrene as imprint resist (Figure 1). Silver island films of 9 nm mass thickness were deposited on the top of the patterned substrates by PVD in a Kurt J. Lesker 4-pocket electron beam evaporation unit. During the film deposition the background pressure was 10^{-6} Torr, and the deposition rate (0.5 Å/s) was monitored with an XTC Inficon quartz crystal oscillator.

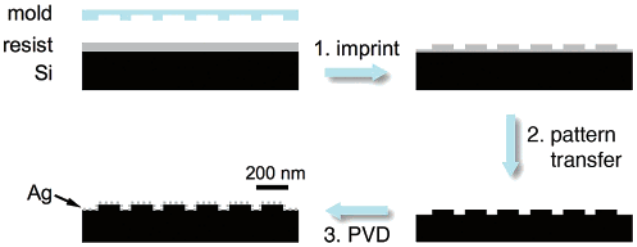

Figure 1. Schematic illustration of the nanoimprint lithography and physical vapor deposition methods used to prepare SERS-active substrates with tunable SPR.

The topography of the Ag films was characterized by high-resolution scanning electron microscopy (SEM, Hitachi S4800) and tapping-mode atomic force microscopy (TM-AFM). AFM measurements were performed on a Digital Instruments Nano-Scope IV operating in tapping mode with n^+-silicon tips (NSC 14 model, Ultrasharp) at a resonant frequency of 256 kHz. All images were collected in high resolution at a scan rate of 0.5 Hz. The data were collected under ambient conditions and each scan was duplicated.

Chemical analysis and oxidation state of the silver thin films were investigated by X-ray photoelectron spectroscopy (XPS) in an Axis 165 XPS (Kratos Analytical). X-ray diffraction (XRD) analysis was carried out on a Bruker D8 Discover, using graphite monochromated Cu Kα radiation ($\lambda = 1.5418$ Å), operated at 40 mA and 40 kV. SPR measurements were performed on a Perkin-Elmer Lambda 35 UV−vis spectrophotometer, using a diffuse reflectance accessory at a 45° angle.

All the vibrational experiments (Raman and SERS) were carried out with 532 and 785 nm excitation laser lines. The inelastically scattered radiation was collected on a Nicolet Almega system equipped with a CCD detector and an optical microscope. Spectra were collected in high-resolution mode with accumulation times ranging from 1 to 10 s. All measurements

* Address correspondence to these authors. H.F.: e-mail hicham.fenniri@ualberta.ca, phone (780) 641-1750. T.V.: e-mail teodor.veres@cnrc-nrc.gc.ca, phone (450) 641−5232.
[†] National Institute for Nanotechnology, National Research Council.
[‡] Industrial Material Institute, National Research Council.
[§] Gunning/Lemieux Chemistry Center, University of Alberta.

10.1021/jp070906s CCC: $37.00
Published on Web 04/19/2007

were made in backscattering geometry, using a 100× microscope objective with a NA value of 0.90, providing scattering areas of 1 μm^2.

Raman spectra of the analytes were directly recorded on the bulk material. Samples for SERS were prepared by casting 2 μL of an ethanolic solution of the analyte (10^{-4} M) on ~5 mm^2 areas of the Ag films (~1 molecule per 20 $Å^2$ on the Ag island film; submonolayer coverage). The 520 cm^{-1} phonon mode of silicon was used as an intensity standard to correct for possible variations of the SERS intensity that are not due to substrate enhancement. The relative enhancement factor (EF) between two different substrates was calculated by applying eq 1:

$$\mathrm{EF} = \frac{I_{\mathrm{Surf.A}} N_{\mathrm{Surf.A}}}{I_{\mathrm{Surf.B}} N_{\mathrm{Surf.B}}} \quad (1)$$

where N represents the number of molecules probed on each substrate and I the SERS intensity. Given that $N_{\mathrm{Surf.A}}$ and $N_{\mathrm{Surf.B}}$ are similar, EF can be reduced to $I_{\mathrm{Surf.A}}/I_{\mathrm{Surf.B}}$.

Results and Discussion

Figure 2 shows scanning electron microscopy and tapping mode atomic force microscopy (TM-AFM) images of the substrates fabricated. Ag island films on flat substrates (AgIF) prepared by physical vapor deposition featured 30−80 nm Ag nanoparticles (average ~32 nm). NIL-patterned substrates featured similar Ag nanoparticle size distribution (30−60 nm, average ~35 nm). Four NIL substrate geometries with a periodicity of 200 nm (Figure 2B−E) and feature height of 120 nm (Figure S1, Supporting Information) were investigated: (a) silver-coated gratings (AgG) of 150 nm separated by 50 nm channels (Figure 2B), (b) 125 × 125 nm^2 silver-coated pillars (AgP12, Figure 2C), (c) 100 × 80 nm^2 silver-coated pillars (AgP10, Figure 2D), and (d) 60 × 40 nm^2 silver-coated pillars (AgP6, Figure 2F).

X-ray photoelectron spectroscopy (XPS) showed a similar composition for all surfaces, regardless of their nanotopographies (Figure 3A, Table 1). The spectra were dominated by Ag 3d bands (374.2, 368.3 eV) typical of metallic Ag, with small amounts of oxygen (1s, 529.8 eV) and carbon (1s, 284.3 eV). Metallic Ag (~75% w/w) was mainly crystalline for all the samples as revealed by X-ray diffraction (Figure 3B).

Remarkably, the SPR spectra varied dramatically with surface topography (Figure 4). The flat substrate (AgIF) featured a strong broad band with a maximum at 482 nm. The SPR for the grated and pillared substrates were significantly red-shifted to 615 (AgG), 660 (AgP12), 718 (AgP10), and 792 nm (AgP6). Since the Ag nanoparticle size, shape, composition, crystallographic properties, and local environment for the three substrates are similar, the red shift was attributed to a combination of short-range static dipolar coupling between nanoparticles[16,17] and long-range retardation effects,[18−20] both the result of variations in surface nanotopography.

The optical enhancement attained on the fabricated surfaces was tested by using dilute solutions of 2-naphthalenethiol (NAT).[21] This analyte was chosen because its electronic absorption maximum at 242 nm (Figure S2, Supporting Information) is far from the laser excitation lines used (532/780 nm), thus eliminating the possibility for surface-enhanced resonance Raman scattering (SERRS) and resulting in identical Raman spectra with both laser lines (Figure S3, Supporting Information). The characteristic SERS spectra of 2-NAT (Figure 5A) were similar regardless of the substrate and laser line used, and were dominated by ring stretching (1621, 1378 cm^{-1}), C−H bending (1080 cm^{-1}), ring deformation, and C−S stretching (364 cm^{-1}) modes. A strong enhancement of the C−S stretching along with the disappearance of the S−H stretching mode (2550, 2560 cm^{-1}) were observed due to the chemisorption of NAT on the Ag nanoparticles (Figure S4, Supporting Information). The fact that the SERS spectra showed the same vibrational features suggests that NAT experiences the same local environment regardless of topographical differences. However, the absolute intensity varied significantly as a function of the SPR position (Figure 5B). Investigation of the SERS intensity of NAT

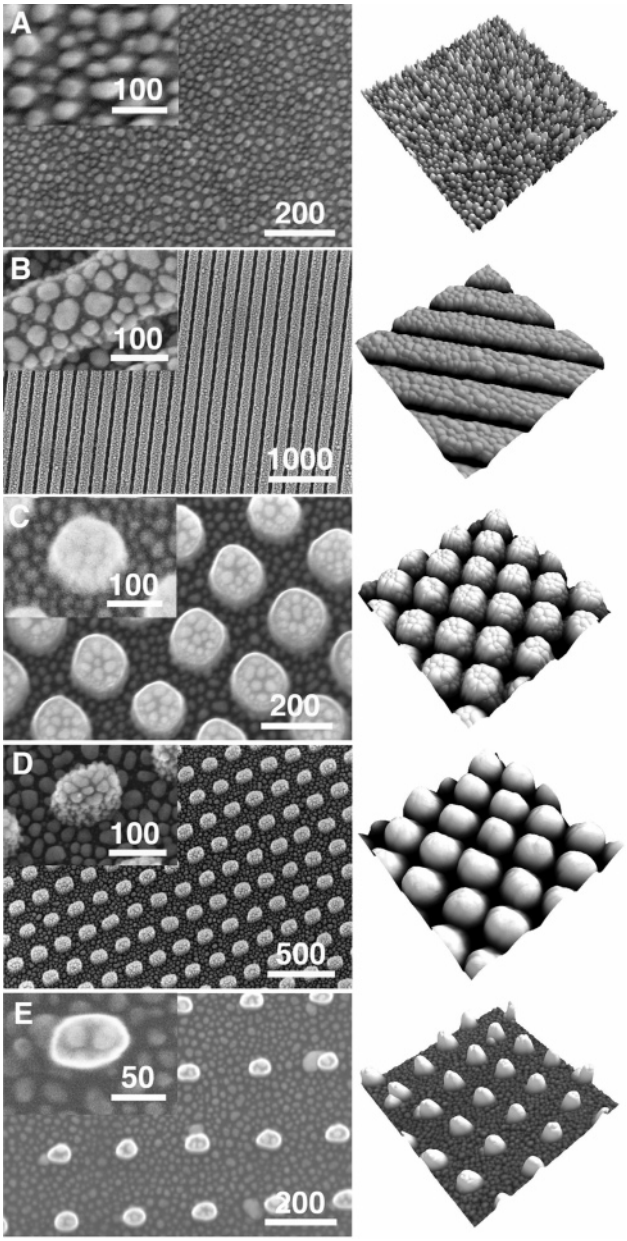

Figure 2. Scanning electron and atomic force micrographs of silver nanoparticles grown by physical vapor deposition on flat (A), grated (B), and pillared (C−E) substrates. The SEM scale bars are in nm, and the AFM scans are 1 × 1 μm^2.

TABLE 1: Chemical Analysis of the Substrates (% Mass Concentration)

element	flat substrate	grated substrate	AgP12	AgP10	AgP6
Ag	75.8	74.8	75.1	73.8	76.2
O	9.16	8.00	8.40	8.10	9.51
C	11.4	13.8	12.3	14.4	13.3

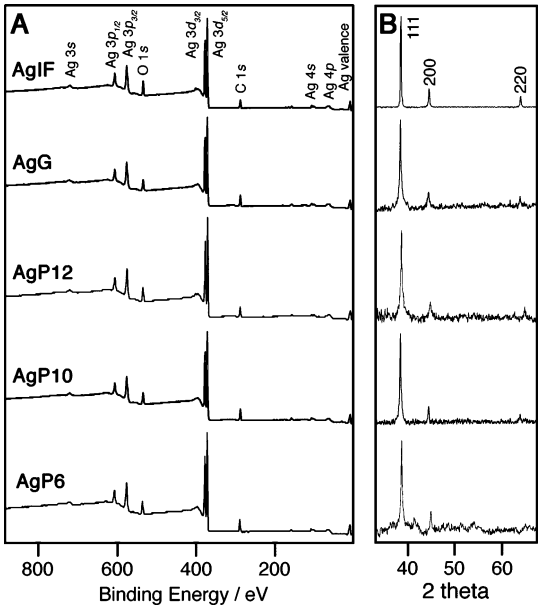

Figure 3. (A) X-ray photoelectron spectra of Ag nanoparticles on flat, grated, and pillared substrates. The spectra demonstrate that the Ag nanoparticles are chemically identical on all three substrates. (B) X-ray diffractograms of Ag nanoparticles on flat (AgIF), grated (AgG), and pillared films (AgP12, AgP10, AgP6). Typical Ag Bragg reflections at d(111), (200), and (220) were indexed to face-centered cubic belonging to the *Fm*3*m* [225] space group (JCPDS file No. 04-0783).

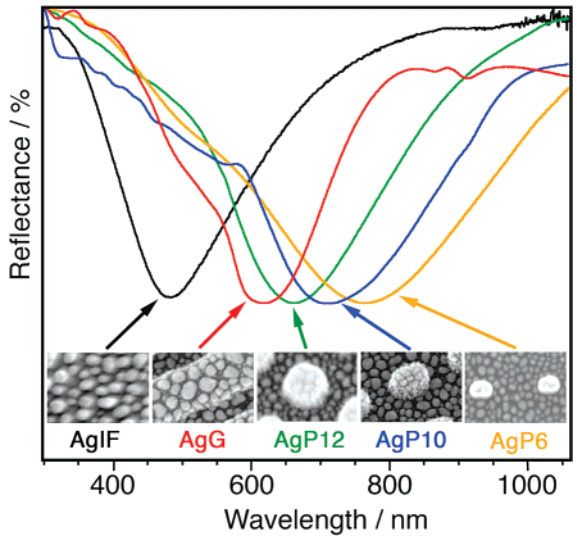

Figure 4. Surface plasmon resonances of Ag-coated flat, grated, and pillared substrates, acquired by diffuse reflectance electronic spectroscopy (45°). Insets are 300 × 200 nm^2.

on the five substrates with the 532 nm laser line showed a substantial increase of the signal with the AgG substrate (SPR $\lambda_{max} = 610$ nm) as compared with AgIF (SPR $\lambda_{max} = 482$ nm). However, the SERS signal decreases from this point onward as the plasmon is red-shifted. When the samples were excited with the 780 nm laser line, the SERS signal increased progressively, reaching a maximum on AgP10 (SPR $\lambda_{max} = 718$). For AgP6 (SPR $\lambda_{max} = 792$) the SERS intensity decreases slightly. All the enhancements observed extended to the entire surface as inferred from the SERS maps (Figure 5C).

The results obtained with NIL substrates are consistent with those previously shown by plasmon[4,11] and wavelength-scanned[5] surface-enhanced Raman excitation spectroscopy. This suggests that the optical enhancement observed on NIL surfaces is due mainly to plasmon coupling, which in turn results from

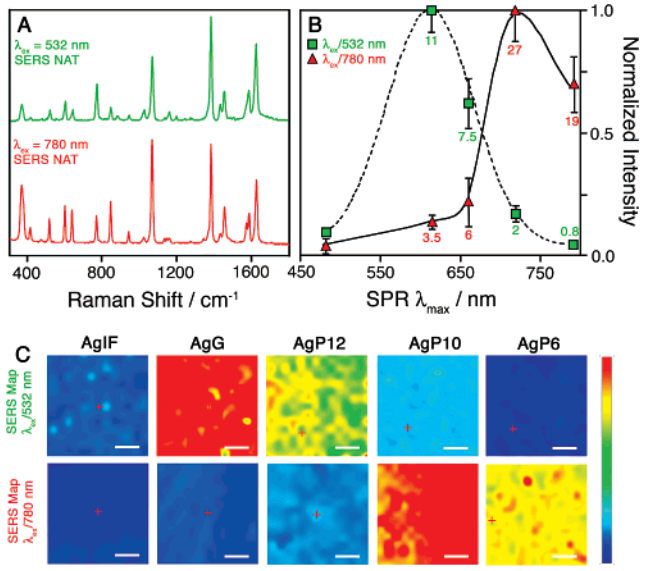

Figure 5. (A) SERS spectra of NAT acquired with 532 and 780 nm laser lines (1 × 10s scan and energy density at the sample of 40 μW). (B) Variation of the intensity of the band at 1378 cm^{-1} for the two lines as a function of the position of the SPR maxima measured under the same experimental conditions. The green and red numbers indicate the enhancement factor obtained for the nanoimprinted substrates (AgG, AgP12, AgP10, AgP6) relative to the flat film (AgIF). (C) SERS mapping of NAT (1378 cm^{-1}, 20 × 20 μm^2, step size 1.5 μm) on the substrates investigated (1 × 3s scan and energy density at the sample of 40 μW).

variations in surface nanotopography. In effect, the SERS spectra of NAT are enhanced for a given laser through optimal coupling between SPR and the incident laser line, whereas the SPR is tuned through the control of the surface topography (pattern and size of the features). Thus NIL appears to be a powerful method for the fabrication of reproducible, large-scale SERS-active substrates with optical tunability. Work is in progress to explore this effect for applications in biosensing and cross-reactive sensor arrays. We are also actively exploring other metal nanoparticles (e.g., gold, silver/gold alloys) to further enhance the optical properties of these surfaces.

Acknowledgment. We thank the National Research Council (NRC) of Canada, the Genomics and Health Initiative, the National Institute for Nanotechnology, the University of Alberta, and the Industrial Materials Institute for supporting this program.

Supporting Information Available: Cross-sectional SEM, electronic and Raman spectra for 2-naphthalenethiol. This material is available free of charge via the Internet at http://pubs.acs.org.

References and Notes

(1) Barnes, W. L.; Dereux, A.; Ebbesen, T. W. *Nature* **2003**, *424*, 824.
(2) Baker, G. A.; Moore, D. S. *Anal. Bioanal. Chem.* **2005**, *382*, 1751.
(3) Moskovits, M. *Rev. Mod. Phys.* **1985**, *57*, 783.
(4) Haynes, C. L.; Van Duyne, R. P. *J. Phys. Chem. B* **2003**, *107*, 7426.
(5) McFarland, A. D.; Young, M. A.; Dieringer, J. A.; Van Duyne, R. P. *J. Phys. Chem. B* **2005**, *109*, 11279.
(6) Schatz, G. C.; Van Duyne, R. P. Electromagnetic mechanism of surface-enhanced spectroscopy. In *Handbook of Vibrational Spectroscopy*; Chalmers, J. M., Griffiths, P. R., Eds.; John Wiley & Sons, Ltd.: Chichester, UK, 2002; Vol. 1, p 759.
(7) Etchegoin, P.; Cohen, L. F.; Hartigan, H.; Brown, R. J. C.; Milton, M. J. T.; Gallop, J. C. *J. Chem. Phys.* **2003**, *119*, 5281.
(8) Kneipp, K.; Wang, Y.; Kneip, H.; Perelman, L. T.; Itzkan, I.; Dasari, R. R.; Feld, M. *Phys. Rev. Lett.* **1997**, *78*, 1667.
(9) Nie, S.; Emory, S. R. *Science* **1997**, *275*, 1102.

(10) Jackson, J. B.; Halas, N. J. *Proc. Natl. Acad. Sci.* **2004**, *101*, 17930.
(11) Alvarez-Puebla, R. A.; Ross, D. J.; Nazri, G.-A.; Aroca, R. F. *Langmuir* **2005**, *21*, 10504.
(12) De Jesus, M. A.; Giesfeldt, K. S.; Oran, J. M.; Abu-Hatab, N. A.; Lavrik, N. V.; J., S. M. *Appl. Spectrosc.* **2005**, *59*, 1500.
(13) Haynes, C. L.; Van Duyne, R. P. *J. Phys. Chem. B* **2001**, *105*, 5599.
(14) Hicks, E. M.; Zhang, X.; Zou, S.; Lyandres, O.; Spears, K. G.; Schatz, G. C.; Van Duyne, R. P. *J. Phys. Chem. B* **2005**, *109*, 22351.
(15) Chou, S. Y.; Krauss, P. R.; Renstrom, P. J. *Appl. Phys. Lett.* **1995**, *67*, 3114.
(16) Murray, C. A.; Bodoff, S. *Phys. Rev. Lett.* **1984**, *52*, 2273.
(17) Lazarides, A. A.; Schatz, G. C. *J. Phys. Chem. B* **2000**, *104*, 460.
(18) Kottmann, J. P.; Martin, O. J. F. *Opt. Lett.* **2001**, *26*, 1096.
(19) Haynes, C. L.; McFarland, A. D.; Zhao, L.; Van Duyne, R. P.; Schatz, G. C.; Gunnarsson, L.; Prikulis, J.; Kasemo, B.; Kall, M. *J. Phys. Chem. B* **2003**, *107*, 7337.
(20) Moran, C. E.; Steele, J. M.; Halas, N. J. *Nano Lett.* **2004**, *4*, 1497.
(21) Alvarez-Puebla, R. A.; dos Santos, D. S., Jr.; Aroca, R. F. *Analyst* **2004**, *129*, 1251.